Supplementary information

Ikkyu Aihara[1,*], Takeshi Mizumoto[2], Takuma Otsuka[2], Hiromitsu Awano[2], Kohei Nagira[2], Hiroshi G. Okuno[2], Kazuyuki Aihara[3]

1 Brain Science Institute, RIKEN, Saitama 351-0198, Japan

2 Graduate School of Informatics, Kyoto University, Kyoto 606-8501, Japan

3 Institute of Industrial Science, The University of Tokyo, Tokyo 153-8505, Japan

∗ **E-mail: ikkyu@brain.riken.jp**

1 Introduction

Numerical simulation of the present mathematical model demonstrates that both two-cluster antisynchronization and wavy antisynchronization are stably observed (Figs.2, 3, and 4 in the paper). To theoretically estimate the stability of these two states, linear stability analysis is provided in Section 2 of this Supplementary information.

In addition, we recorded frog choruses at an actual paddy field by using our sound-imaging method [1], and detected two-cluster antisynchronization several times (Fig.7 and Table 1). All the other observation data are shown in Section 3 of this Supplementary information, so as to represent the details of the spatio-temporal patterns in different choruses.

2 Theoretical Analysis

We perform linear stability analysis on the following two cases: (1) two-cluster antisynchronization and wavy antisynchronization at a circular field, and (2) two-cluster antisynchronization at a straight-line field.

Numerical simulation shows that two-cluster antisynchronization and wavy antisynchronization are stably observed at a circular field, where frogs are positioned along the edge at the same interval (Figs.2 and 3). This is the most fundamental case of bistability of the two states in our model.

On the other hand, field observations revealed the dominant occurrence of two-cluster antisynchronization at an actual field (Table 1). During the field observations, sound-imaging devices *Fireflies* covered one edge of a rectangular field along which considerably larger number of frogs were calling (see Methods and Fig.6C). Moreover, our model reproduces two-cluster antisynchronization when assuming a straight-line field (Fig.4B at $L_x = 60$). Thus, two-cluster antisynchronization at such straight-line distribution of the frogs is common to the numerical simulation and field observations.

2.1 Assumption of Spatial Distribution

Let us fix positions of calling frogs along the edge of a circular or straight-line field, so as to simply reproduce the results of the numerical simulation (Figs.2A, 3A, and 4). First, the position of the nth frog ($n = 1, 2, ..., N$) at a circular field is described as follows, for simplicity:

$$\boldsymbol{r}_n = L \begin{pmatrix} \cos\delta_n \\ \sin\delta_n \end{pmatrix}, \tag{S1}$$

where $\delta_n \pmod{2\pi}$ represents the angle from the center of a circular field to the nth frog that is fixed on the edge of the field, and is given by $\delta_n = \frac{2\pi(n-1)}{N}$. The parameter L represents the radius of the field (Fig.S1A). Consequently, the distance between the nth and mth frogs at the circular field is given by

$$d_{n,m} = |\boldsymbol{r}_n - \boldsymbol{r}_m| = 2L|\sin(\frac{\delta_m - \delta_n}{2})|, \tag{S2}$$

where $d_{n,m} = d_{m,n}$ is satisfied.

Second, the position of the nth frog ($n = 1, 2, ..., N$) at a straight-line field is described as follows, for simplicity:

$$\boldsymbol{r}_n = L_x \begin{pmatrix} (n-1)/(N-1) \\ 0 \end{pmatrix}, \tag{S3}$$

where the parameter L_x represents the length of the field (Fig.S1B). Consequently, the distance between the nth and mth frogs ($n \neq m$) at the straight-line field is given by

$$d_{n,m} = L_x \frac{|n-m|}{N-1}, \tag{S4}$$

where $d_{n,m} = d_{m,n}$ is satisfied.

2.2 Definition of Two-cluster and Wavy Antisynchronization

To define two-cluster and wavy antisynchronization, we introduce a phase difference between the nth and 1st frogs ($n = 2, 3, ..., N$) as follows:

$$\phi_{n,1} \equiv \theta_n - \theta_1 (\mathrm{mod}\ 2\pi). \tag{S5}$$

By using $\phi_{n,1}$, two-cluster antisynchronization is defined by

$$\phi_{n,1} = \begin{cases} \pi & (\text{if } n \text{ is even}), \\ 0 & (\text{if } n \text{ is odd}). \end{cases} \tag{S6}$$

In addition, wavy antisynchronization is defined by

$$\phi_{n,1} = \begin{cases} \pi - \frac{2k\pi(n-1)}{N} & (\text{if } n \text{ is even}), \\ -\frac{2k\pi(n-1)}{N} & (\text{if } n \text{ is odd}). \end{cases} \tag{S7}$$

where an integer k represents the wave number of wavy antisynchronization. Equation (S7) is consistent with the description of wavy antisynchronization shown in the paper, i.e., $\theta_n - \theta_{n+1} = \pi + \frac{2k\pi}{N}$ ($n = 2, 3, ..., N$).

2.3 Mathematical Frameworks of Linear Stability Analysis

We derive an equation for linear stability analysis based on the present mathematical model. From equations (5), (7) and (S5), the differential equation for $\phi_{n,1}$ ($n = 2, 3, ..., n$) is given as follows:

$$\frac{d\phi_{n,1}}{dt} = \frac{d\theta_n}{dt} - \frac{d\theta_1}{dt} \tag{S8}$$

$$= \sum_{m=1, m\neq n}^{N} \frac{K}{d_{n,m}^2} \sin(\phi_{n,1} - \phi_{m,1}) + \sum_{m=2}^{N} \frac{K}{d_{m,1}^2} \sin \phi_{m,1}, \tag{S9}$$

$$= \frac{K}{d_{n,1}^2} \sin \phi_{n,1} + \sum_{m=2, m\neq n}^{N} \frac{K}{d_{n,m}^2} \sin(\phi_{n,1} - \phi_{m,1}) + \sum_{m=2}^{N} \frac{K}{d_{m,1}^2} \sin \phi_{m,1}, \tag{S10}$$

where we assume the identical angular velocity $\omega_n = \omega$ to every frogs and also $K_{nm} = K$ for all n and m with $n \neq m$, according to the assumption of the numerical simulation in the paper (Figs.2, 3, 4 and 5). Then, we introduce a small perturbation around a stable equilibrium state as follows:

$$\phi_{n,1} = \phi_{n,1}^* + \delta\phi_{n,1}, \tag{S11}$$

where $\phi_{n,1}^*$ represents a stable equilibrium state of $\phi_{n,1}$ satisfying $\frac{d\phi_{n,1}}{dt}|_{\phi_{2,1}=\phi_{2,1}^*, \phi_{3,1}=\phi_{3,1}^*, ...} = 0$, and $\delta\phi_{n,1}$ represents the perturbation. Substituting equation (S11) to equation (S10) yields the following

linear approximation dynamics of $\delta\phi_{n,1}$:

$$\begin{aligned}\frac{d}{dt}\delta\phi_{n,1} \simeq &\left[\frac{2K}{d_{n,1}^2}\cos\phi_{n,1}^* + \sum_{m=2,m\neq n}^{N}\frac{K}{d_{n,m}^2}\cos(\phi_{n,1}^*-\phi_{m,1}^*)\right]\delta\phi_{n,1} \\ &+ \sum_{m=2,m\neq n}^{N}\left[-\frac{K}{d_{n,m}^2}\cos(\phi_{n,1}^*-\phi_{m,1}^*) + \frac{K}{d_{1,m}^2}\cos\phi_{m,1}^*\right]\delta\phi_{m,1}.\end{aligned} \tag{S12}$$

By using equation (S12), $(N-1)\times(N-1)$ matrix A, and the vector $\delta\boldsymbol{\phi} = (\delta\phi_{2,1},\ \delta\phi_{3,1},\ ...,\ \delta\phi_{N,1})^\top$, the differential equation of $\delta\boldsymbol{\phi}$ is described as follows:

$$\frac{d}{dt}\delta\boldsymbol{\phi} = A\delta\boldsymbol{\phi}, \tag{S13}$$

where the entry in the nth row and the mth column of A is given by

$$A_{n,m} = \begin{cases} \frac{2K}{d_{n,1}^2}\cos\phi_{n,1}^* + \sum_{j=2,j\neq n}^{N}\frac{K}{d_{n,j}^2}\cos(\phi_{n,1}^*-\phi_{j,1}^*) & (\text{if } n=m), \\ -\frac{K}{d_{n,m}^2}\cos(\phi_{n,1}^*-\phi_{m,1}^*) + \frac{K}{d_{1,m}^2}\cos\phi_{m,1}^* & (\text{if } n\neq m). \end{cases} \tag{S14}$$

2.4 Linear Stability Analysis on the Case of the Circular Distribution

Let us analyze linear stability of two-cluster antisynchronization and wavy antisynchronization, when assuming the circular distribution of frogs described by equation (S1).

First, we examine linear stability of two-cluster antisynchronization. Equation (S6) satisfies both $\sin\phi_{n,1} = 0$ and $\sin(\phi_{n,1}-\phi_{m,1}) = 0$ in equation (S10), so that two-cluster antisynchronization defined by equation (S6) is an equilibrium state at the circular distribution. Then, we substitute equations (S2) and (S6) to equation (S14), and calculate eigenvalues of the matrix A on the assumption of $L = 20$, $N = 20$ and $K = 1$. Note that these are the same parameter values with the numerical simulation shown in the paper. Figure S2A represents the eigenvalues which are estimated by using the *eig* function of MATLAB [2]. It is shown that all the eigenvalues are real, and the maximum eigenvalue is negative. Therefore, the two-cluster antisynchronization is asymptotically stable.

Second, we examine linear stability of wavy antisynchronization. At the circular distribution, the distance between the nth and $(n+m)$th frogs is the same with that between the nth and $(n-m)$th frogs, so that $d_{n,n+m} = d_{n,n-m}$ is satisfied (see Fig.S1A and also equation (S2)). When N is even, equation (S9) is rewritten as follows:

$$\begin{aligned}\frac{d}{dt}\phi_{n,1} =& \frac{K}{d_{n,n+N/2}^2}\sin(\phi_{n,1}-\phi_{n+N/2,1}) + \sum_{m=1}^{N/2-1}\frac{K}{d_{n,n+m}^2}\big[\sin(\phi_{n,1}-\phi_{n+m,1}) + \sin(\phi_{n,1}-\phi_{n-m,1})\big] \\ &+ \frac{K}{d_{1,N/2+1}}\sin\phi_{N/2+1,1} + \sum_{m=1}^{N/2-1}\frac{K}{d_{1,1+m}^2}\big[\sin\phi_{1+m,1} + \sin\phi_{1-m,1}\big],\end{aligned} \tag{S15}$$

where a subscript m attached like $d_{j,m}$ and $\phi_{m,1}$ means m (mod N) for $m < 1$ and $m > N$. Equation (S7) satisfies $\sin(\phi_{n,1}-\phi_{n+N/2,1}) = 0$, $\sin(\phi_{n,1}-\phi_{n+m,1}) + \sin(\phi_{n,1}-\phi_{n-m,1}) = 0$, $\sin\phi_{N/2+1,1} = 0$, and $\sin\phi_{1+m,1} + \sin\phi_{1-m,1} = 0$ in equation (S15). Therefore, wavy antisynchronization defined by equation (S7) is an equilibrium state when assuming the circular distribution and even N. Then, we substitute equations (S2) and (S7) to equation (S14), and numerically calculate eigenvalues of the matrix A on the assumption of $L = 20$, $N = 20$ and $K = 1$. It is shown that all the eigenvalues are real, and the maximum eigenvalue is negative (Fig.S2B). Therefore, the wavy antisynchronization is asymptotically stable.

2.5 Linear Stability Analysis on the Case of the Straight-Line Distribution

We analyze linear stability of two-cluster antisynchronization when assuming the straight-line distribution described by equation (S3). Equation (S6) satisfies both $\sin\phi_{n,1} = 0$ and $\sin(\phi_{n,1} - \phi_{m,1}) = 0$ in equation (S10), so that two-cluster antisynchronization defined by equation (S6) is an equilibrium state at the straight-line distribution. Then, we substitute equations (S4) and (S6) to equation (S14), and numerically calculate eigenvalues of the matrix A on the assumption of $L_x = 60$, $N = 20$ and $K = 1$. Note that these are the same parameter values with the numerical simulation shown in the paper. The analysis has shown that all the eigenvalues are real, and the maximum eigenvalue is negative (Fig.S2C). Therefore, the two-cluster antisynchronization is asymptotically stable.

3 Other Experimental Results

Figures S3 – S6 represent the light patterns of the LEDs attached to sound-imaging devices *Fireflies* and also the time series data of the order parameters, which were obtained from the field observations on 12th, 14th, 16th, and 17th June in 2011, respectively. The order parameter $R_{cluster}$ mostly took larger values than R_{wavy} and R_{in}.

On the other hand, Figure S7 represents the light pattern recorded on 11th June in 2011. Because too many frogs called at the paddy field on this day, we could not precisely estimate calling times and positions of the frogs from this data.

References

1. Mizumoto, T., Aihara, I., Otsuka, T., Takeda, R., Aihara, K., Okuno, H.G. Sound imaging of nocturnal animal calls in their natural habitat, *J. Comp. Physiol. A* **197**, 915-921 (2011).

2. http://www.mathworks.com/help/symbolic/eig.html

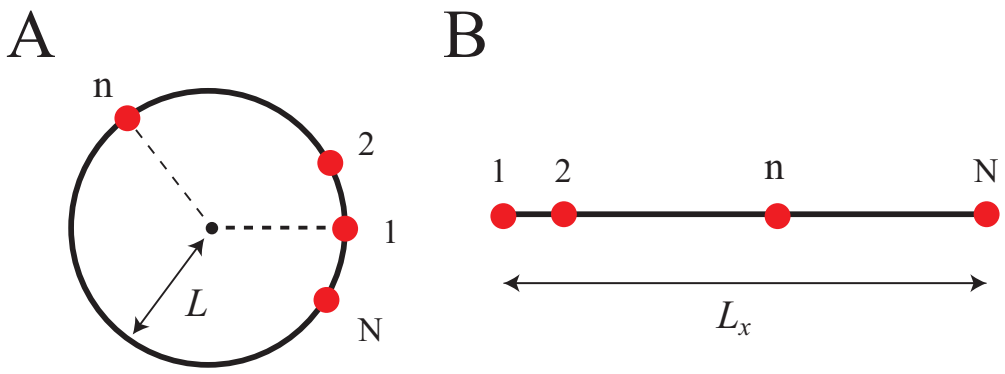

Figure S1. Spatial distributions of calling frogs that are assumed for linear stability analysis: (A) the distribution at a circular field, and (B) the distribution at a straight-line field. To simply replicate the spatial distribution detected by the numerical simulation, we assume that the positions of calling frogs are restricted on the edges of the fields. In the case of a circular field, the parameter L represents the radius of the field. In the case of a straight-line field, the parameter L_x represents the length of the field.

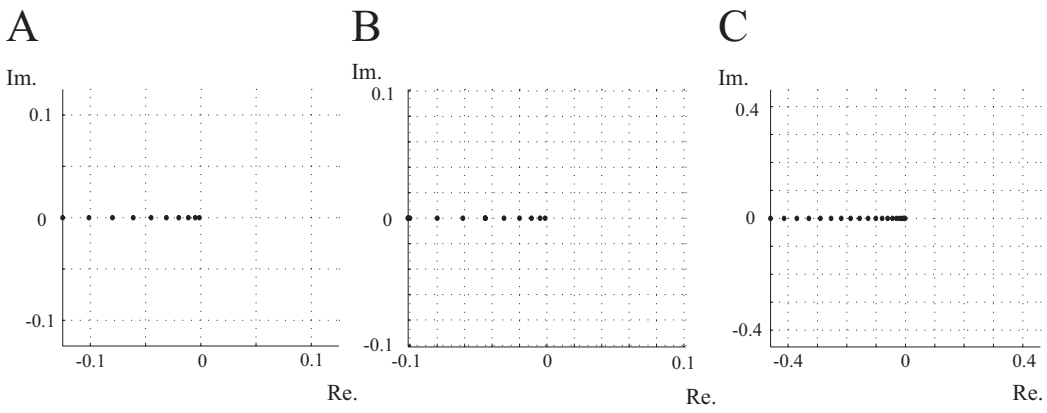

Figure S2. Linear stability analysis on the three states: (A) two-cluster antisynchronization at the circular distribution, (B) wavy antisynchronization at the circular distribution, and (C) two-cluster antisynchronization at the straight-line distribution. The vertical axis represents the imaginary part of the eigenvalues, and the horizontal axis represents the real part. In this analysis, we used the same parameter values with the numerical simulation shown in the paper, i.e., $L = 20$, $L_x = 60$, $N = 20$ and $K = 1$. The analysis demonstrates that the imaginary parts of all the eigenvalues are 0, and that the maximum eigenvalues of States (A), (B) and (C) are -0.0012, -0.0012 and -0.0013, respectively. This means that the equilibrium states of (A)–(C) are asymptotically stable at the present parameter values.

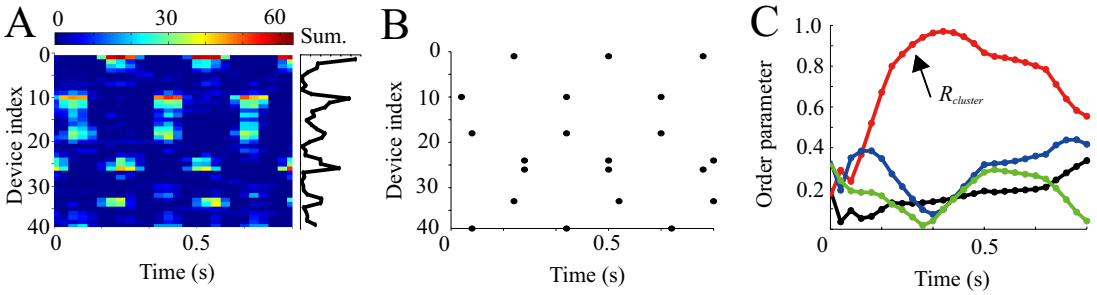

Figure S3. Spatio-temporal structure in an actual frog chorus recorded on 12th June in 2011. (A) A light pattern of sound-imaging devices deployed at the paddy field. While the horizontal and vertical axes represent the time and device index, the colored plots represent the light intensities of the devices. The attached right panel gives the summation of the light intensity of each device. (B) Calling times and positions of male Japanese tree frogs. Each black dot represents the calling times and positions of the frogs. (C) Time series data of the order parameters, $R_{cluster}$, R_{wavy}, and R_{in}. Red, blue, green, and black lines represent the time series data of $R_{cluster}$, R_{wavy} for $k = 1$ and $k = -1$, and R_{in}, respectively. $R_{cluster}$ mostly took much larger values than R_{wavy} and R_{in}.

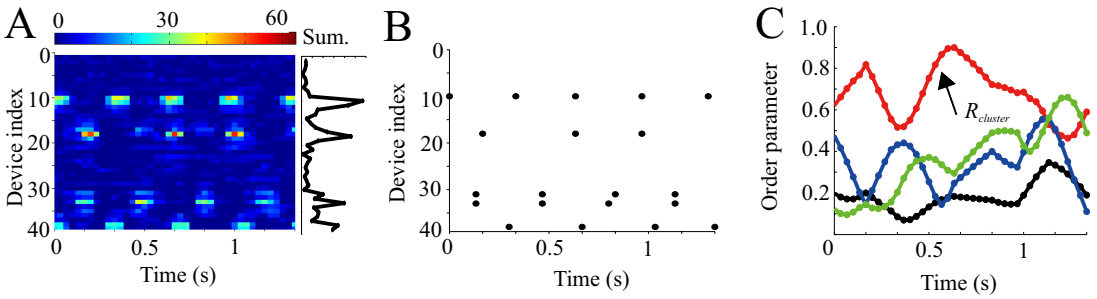

Figure S4. Spatio-temporal structure in an actual frog chorus recorded on 14th June in 2011. (A) A light pattern of sound-imaging devices deployed at the paddy field. (B) Calling times and positions of male Japanese tree frogs. (C) Time series data of the order parameters, $R_{cluster}$, R_{wavy} for $k = 1$ and $k = -1$, and R_{in}. $R_{cluster}$ mostly took much larger values than R_{wavy} and R_{in}.

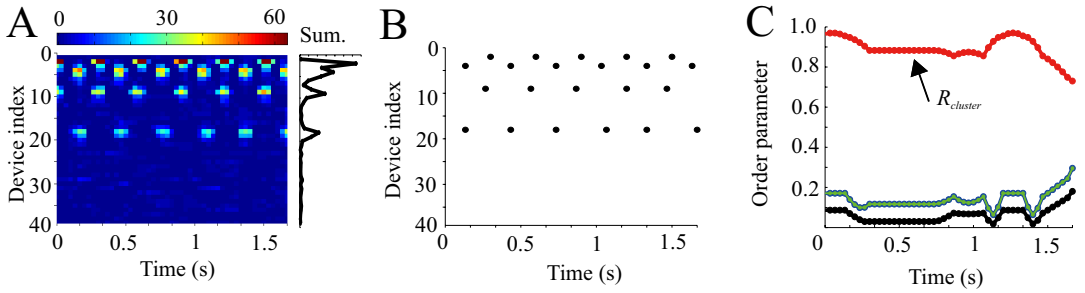

Figure S5. Spatio-temporal structure in an actual frog chorus recorded on 16th June in 2011. (A) A light pattern of sound-imaging devices deployed at the paddy field. (B) Calling times and positions of male Japanese tree frogs. (C) Time series data of the order parameters, $R_{cluster}$, R_{wavy} for $k = 1$ and $k = -1$, and R_{in}. $R_{cluster}$ stably took much larger values than R_{wavy} and R_{in}. In this data, R_{wavy} for $k = 1$ and R_{wavy} for $k = -1$ overlap each other.

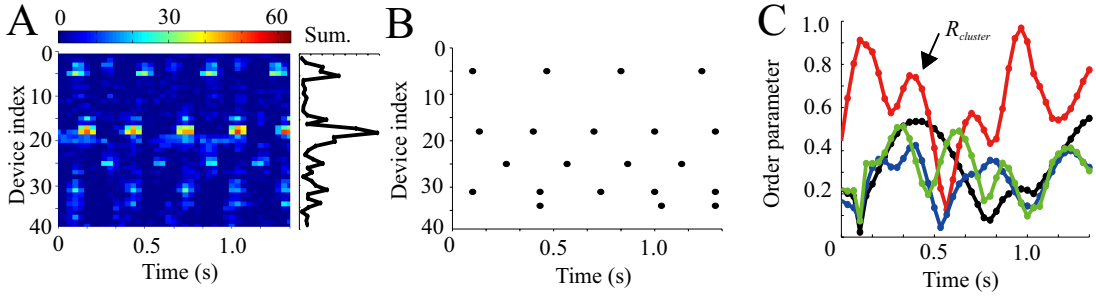

Figure S6. Spatio-temporal structure in an actual frog chorus recorded on 17th June in 2011. (A) A light pattern of sound-imaging devices deployed at the paddy field. (B) Calling times and positions of male Japanese tree frogs. (C) Time series data of the order parameters, $R_{cluster}$, R_{wavy} for $k = 1$ and $k = -1$, and R_{in}. $R_{cluster}$ temporally took much larger values than R_{wavy} and R_{in}.

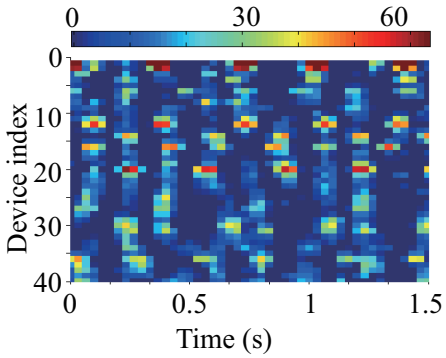

Figure S7. A light pattern of sound-imaging devices deployed at the paddy field, which was recorded on 11th June in 2011. This data set suggested that there were so many calling frogs at the paddy field, and then the light pattern was very complicated. Because we could not precisely estimate the calling times and positions of the frogs, we did not use this data for the calculation of the order parameters.